AIAA JOURNAL
Vol. 43, No. 10, October 2005

Tip Vortex Behind a Wing Undergoing Deep-Stall Oscillation

D. Birch* and T. Lee†
McGill University, Montreal, Quebec H3A 2K6, Canada

The flow structure of a tip vortex in the near field of a NACA 0015 wing with an effective aspect ratio of 5.04 undergoing a deep-stall oscillation with $\alpha(t) = 18\ \text{deg} + 6\ \text{deg} \sin \omega t$ at $Re = 1.86 \times 10^5$ was investigated. The wing oscillation imposed a strong discrepancy in contour shapes and magnitudes between the pitch-up and pitch-down phases of the oscillation cycle. The vortex was more organized and nearly axisymmetric for $x/c > 0.5$ during pitch-up than during pitch-down. The peak tangential velocity and vorticity and the strength and size of the vortex increased with $\alpha(t)$, except in the vicinity of $\alpha_{\max}$, and had higher values during pitch-up than during pitch-down. The axial flow was always wake like and the velocity deficit decreased with $\alpha(t)$, while exhibiting a sharp increase and decrease on the upstroke and downstroke in the vicinity of $\alpha_{\max}$, respectively. The tangential velocity decreased slightly with the downstream distance. The vortex size increased rather significantly with x/c during pitch-down while remaining virtually unchanged during pitch-up. The inner region of the vortex exhibited a self-similar structure, similar to that of a stationary wing. The induced drag increased with $\alpha(t)$ and had a local maximum at 20 deg during pitch-up.

Nomenclature

AR	=	aspect ratio, $= b^2/S$
b	=	(semi-) wing span
C_{Di}	=	induced drag coefficient, $= D_i/\frac{1}{2}\rho u_\infty^2 S$
C_l	=	section lift coefficient
c	=	airfoil chord
D_i	=	induced drag
f	=	oscillation frequency
Re	=	chord Reynolds number, $= u_\infty c/\nu$
r	=	radial distance from vortex center
r_c	=	core radius at which $v_\theta = v_{\theta\,\max}$
r_o	=	vortex outer radius
S	=	wing area
t	=	time
u	=	axial velocity
u_∞	=	freestream velocity
u'	=	rms axial turbulence
v	=	transverse mean velocity
v_θ	=	tangential or swirl velocity
w	=	spanwise mean velocity
x	=	streamwise or axial distance
y	=	transverse distance
z	=	spanwise distance
α	=	angle of attack
α_{ss}	=	static-stall angle
Γ	=	circulation or vortex strength
Γ_b	=	bound circulation
Γ_c	=	core circulation
Γ_0	=	total circulation
ζ	=	streamwise vorticity
κ	=	reduced frequency, $= \pi f c/u_\infty$
ν	=	kinematic viscosity
ρ	=	density
σ	=	source term in Eq. (4)
ϕ	=	velocity potential
ψ	=	stream function

Subscripts

d	=	pitch-down
u	=	pitch-up

Received 30 August 2004; revision received 19 April 2005; accepted for publication 8 May 2005.

*Ph.D. Research Assistant, Department of Mechanical Engineering.
†Associate Professor, Department of Mechanical Engineering. Member AIAA.

I. Introduction

THE counter-rotating longitudinal vortices generated by aircraft wing tips, because of their hazardous effects on flight safety and airport capacity, continue to be of concern to the aviation industry and aircraft manufacturers alike. The near-field flow characteristics of a tip vortex also play a significant role in the understanding and control of blade-vortex-interaction noise and vibration of rotorcraft and are strongly affected by the complex retreating-blade dynamic-stall flow phenomena (which impose high-speed limitations of modern helicopters). The phenomenon of dynamic stall on airfoils and lifting surfaces in unsteady flow environments has been recognized and studied for many years, both as an important practical problem and as a challenging fundamental one as well. Extensive experimental and computational investigations[1–6] have been conducted to investigate the dynamic-stall flow phenomena developed on an oscillating airfoil. It is now known that the predominant feature of dynamic stall is the formation, convection, and shedding over the airfoil upper surface of a vortex-like disturbance, that is, the leading-edge vortex (LEV), from the leading edge of the airfoil, which induces a nonlinearly fluctuating pressure field and produces transient variations in forces and moments that are fundamentally different from their steady-state counterparts. After the energetic LEV passes off the trailing edge, the flow progresses to a state of full separation over the upper surface and is accompanied by a sudden loss of lift and increase in the negative pitching moment (Fig. 1). Furthermore, if and when the angle of attack α becomes low enough, the flow will finally reattach again from the leading edge. An excellent review is given by McCroskey.[3] Most recently, the spatial-temporal progression of the critical boundary-layer flow points (including the locations of transition, flow reversal and separation, and reattachment and relaminarization points) and also the behavior of the LEV were measured and characterized nonintrusively by Lee and coworkers[5,6] by using closely spaced multiple hot-film sensor (MHFS) arrays.

Lee and coworkers quantified that for a NACA 0012 airfoil (hinged at quarter-chord location) subjected to deep-stall oscillations at $Re = 1.35 \times 10^5$ the prior-to-stall boundary-layer conditions were dominated by the approximated linear upward spread of a trailing-edge turbulent flow reversal (always up to an uppermost of $s/c = 0.26$; s is the surface distance from the leading edge of the airfoil, and c is the airfoil chord), and the sudden turbulent breakdown at around $s/c = 0.14$, and the subsequent formation and

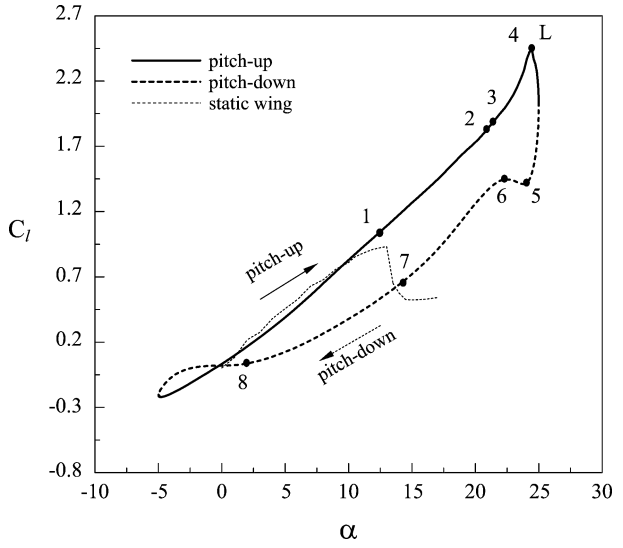

Fig. 1 Dynamic lift loop for a NACA 0012 airfoil oscillated with $\alpha(t) = 10 \text{ deg} + 15 \text{ deg} \sin \omega t$ at $\kappa = 0.1$ and $Re = 1.35 \times 10^5$. Points 1 and 2 correspond to the onset and end of the upward spread flow reversal; points 3 and 4 indicate the occurrence of the turbulent breakdown and the subsequent initiation, growth, and convection of the LEV; point 4 denotes LEV detachment and lift stall; points 4 and 5 indicate that the lift coefficient underwent a sharp drop as soon as the LEV passed off the trailing edge and the airfoil remained fully stalled. At point 6, there was a slight increase in C_l because of the presence and convection of the secondary vortex; points 6 and 7 indicate the fully separated flow. Points 7 and 8 denote the beginning and completion of the flow reattachment. *L* is the lift stall. (Figure reproduced from Lee and Gerontakos.[6])

convection of an energetic LEV. The LEV and the secondary vortex always spread rearward at 45 and 30% of the freestream velocity u_∞, respectively, insensitive to the reduced frequency. The lift stall occurred when the LEV reached about 90% of the chord, whereas the moment stall occurred at the sudden turbulent breakdown. They also reported that the observed hystereses in the dynamic airload and moment loops were mainly attributed to the hysteresis, in terms of phases and α, observed between the unsteady flow separation and reattachment points. Furthermore, by correlating the MHFS signals with the dynamic-load loops the variations in the C_l-α curve, especially the stall angle delay and the lift increment prior to, during, and after the stall, were characterized and quantified (Fig. 1). Note that the unsteady boundary-layer and stall events observed on a NACA 0012 airfoil are fundamentally similar to that of a NACA 0015 airfoil. It is believed that the observed various unsteady boundary-layer and stall events of an oscillating airfoil will also have a significant influence on the flow structure of the tip vortex thus generated. So far, only three refereed experimental investigations,[7–9] to the author's knowledge, with a limited frequency and amplitude range had been reported.

Freymuth et al.[7] pioneered the investigation of the near-field wing-tip vortex behind an oscillating delta wing for $0 < x/c < 1$ by using flow-visualization studies and found that the flow in this region was highly three dimensional and exhibited strong spatial velocity gradients (x is the distance downstream of the wing trailing edge). Ramaprian and Zheng[8] studied the near field of the tip vortex behind an oscillating NACA 0015 rectangular wing with a square tip by using a three-component laser Doppler anemometer at $Re = 1.8 \times 10^5$ with $\alpha(t) = 10 \text{ deg} + 5 \text{ deg} \sin(2\pi f t)$ (i.e., the light-stall oscillation case[3,6]) and $\kappa (= \pi f c/u_\infty$, where f is the oscillation frequency and t is the time) $= 0.1$. They explored the unsteady velocity and vorticity fields associated with the evolving tip vortex in the near field for $0.16 < x/c < 2.66$ and observed that the average trajectory of the oscillating tip vortex was very nearly the same as for a stationary wing at the mean incidence. They also reported that the length and circulation scales, as well as the maximum circulation carried by the vortex flow under the conditions studied, were modulated in a significantly nonquasisteady manner. The normalized circulation distribution across most of the inner part of the vortex for $x/c > 0.7$, however, exhibited the same universal behavior as the vortex behind a stationary wing. More recently, Chang and Park[9] examined the hysteretic behavior of the wake behind a NACA 0012 airfoil oscillated with $\alpha(t) = 15 \text{ deg} + 15 \text{ deg} \sin \omega t$ (i.e., the deep-stall oscillation case[3,6]) at $\kappa = 0.09$ for $Re = 3.4 \times 10^4$ by using a triple hot-film probe at $x/c = 0.5$ and 1.5. Chang and Park found that the size of the vortex core was larger, and the peak tangential velocity and the axial velocity deficit were smaller during pitch-down than during pitch-up. Also, because of the massive LEV flow separation, the circulation or vortex strength of the tip vortex at a given α was greater during pitch-up than during pitch-down. The details of the vortex flow characteristics, however, were not reported.

In summary, it is now well known that wing oscillations lead to the complex unsteady flow phenomena and the large variations in the dynamic airloads; however, much work is still needed to better understand and control the tip vortex generated behind an oscillating wing under the influence of different frequencies and amplitudes. The objective of this study was to characterize the downstream development of the three-dimensional flow structure of a tip vortex in the near field ($x/c = 0.5$–3) behind a square-tipped, rectangular NACA 0015 wing subjected to deep-stall oscillation at $Re = 1.86 \times 10^5$ by using a triple hot-wire probe. Special attention was given to the spatial-temporal behavior of the phase-locked ensemble-averaged crossflow and axial velocity fields, the turbulence structure, and the strength, size, and trajectory (a measure of the effective span) of the vortex, compared to the stationary-wing values, over one cycle of oscillation at selected downstream distances. Lift-induced drag coefficients were also computed.

II. Experimental Apparatus and Methods

The experiment was carried out in the $0.9 \times 1.2 \times 2.7$ m suction-type subsonic wind tunnel at McGill University with a freestream turbulence intensity of 0.03% at 35 m/s. A square-tipped, rectangular NACA 0015 wing with a chord of 20.3 cm, a span b of 50.8 cm, and an aspect ratio ARof 2.5 was used to generate the tip vortex (Fig. 2a). The wing model was mounted horizontally at the center

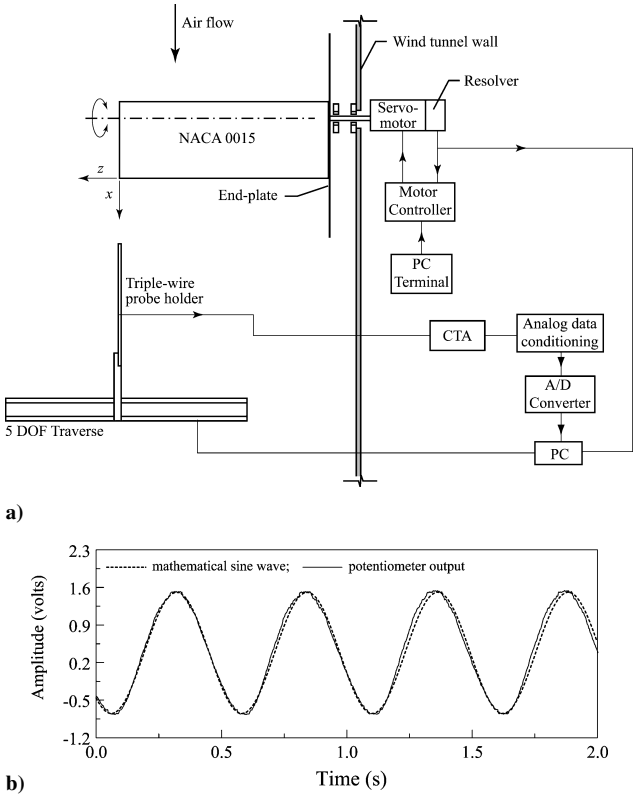

Fig. 2 Schematic of a) oscillating-wing experimental setup and b) sinusoidal output wave forms.

of the sidewall of the wind-tunnel test section. A $0.48 \times 60 \times 60$ cm aluminum endplate with sharp leading edges was fixed to the sidewall of the test section. The gap between the wing and the endplate was kept at less than 1 mm to minimize the leakage flow through the gap. The origin of the coordinate system was located at the trailing edge of the wing tip with the x, y, and z axes in the streamwise, transverse, and spanwise directions, respectively. A servomotor was used to provide the sinusoidal motions at various oscillation amplitudes and frequencies of the wing about its quarter-chord. The mean incidence of the oscillation was set at 18 deg with the amplitude fixed at 6 deg. The reduced frequency was set at $\kappa = 0.09$. The oscillation frequency was measured to an accuracy of ± 0.02 Hz. Information on the phase angle and instantaneous direction of the wing motion (i.e., pitch-up or pitch-down) during the oscillation cycle was obtained from both the servomotor feedback resolver and a potentiometer mounted on the servomotor shaft. Figure 2b shows the typical sinusoidal outputs compared with a mathematically generated sine-wave form. Note that when the phase angle was within the range $0 \le \tau \le 0.5\pi$ (or $0 \le \tau \le 90$ deg) and $1.5\pi \le \tau \le 2\pi$ (or 270 deg $\le \tau \le 360$ deg) the airfoil was described to be in pitch-up; when $0.5\pi \le \tau \le 1.5\pi$ (or 90 deg $\le \tau \le 270$ deg), the airfoil was said to be in pitch-down. Also, in the following discussion the suffix u is used to indicate pitch-up when α is increasing and d is used to indicate pitch-down when α is decreasing. The instantaneous velocities were subsequently ensemble averaged over 40–80 oscillating cycles to obtain phased-locked averages of the flow properties at various phase positions during the cycle. A miniature triple hot-wire probe (Auspex Model AVEP-3-102 with a measurement volume of 0.5 mm^3) was used to measure the mean and fluctuating velocity components. The mean flowfields behind the stationary wing were also examined by using a seven-hole pressure probe (with an outside diameter of 2.4 mm). The pressure probe and triple hot-wire probe were calibrated in situ, following the calibration procedures described by Wenger and Devenport[10] and Chow et al.,[11] respectively, before the installation of the model. The pressure and hot-wire signals were sampled at 500 Hz and were recorded on a PC through a 16-bit A/D converter board. Probe traversing was achieved through a custom-built computer-controlled traversing system with a position resolution in all three directions of 20 μm. The three-dimensional velocities downstream of the trailing edge of the wing were measured in planes perpendicular to the freestream velocity at six downstream locations: $x/c = 0.5$, 1.0, 1.5, 2, 2.5, and 3.0. Data planes taken in the near field of the wing models had 46×46 measuring grid points with an increment of $\Delta y = \Delta z = 3.2$ mm. The freestream velocity was fixed at 14.4 m/s, which rendered a chord Reynolds number of 1.86×10^5.

The maximum experimental uncertainties in the results reported have been estimated as follows[12]: mean velocity 3.5%, vorticity component 8%, vortex radius 4%, and velocity fluctuation 3%. No wind-tunnel wall corrections were made to the present measurements. Furthermore, it is known that the lateral excursions to which a trailing vortex is prone when situated in a freestream containing ambient turbulence have long caused problems in measurement of vortex characteristics and that the meander amplitude is linearly proportional to the level of freestream turbulence and to the downstream distance from the generating lifting surface. In the present low-turbulence wind tunnel, the meander amplitude was greatly reduced because of the reduction in stream turbulence. However, the vortex meandering in the near field behind the generating wing was examined by using the correlation technique/criteria employed by Chow et al.[11] The meandering of the vortex was determined to be small and did not contribute appreciably to the present measurements.

III. Results and Discussion

A. Phase-Locked Ensemble-Averaged Vortex Flow Characteristics

The overall flow structure of the tip vortex (in terms of the phase-locked ensemble-averaged streamwise mean vorticity $\zeta c/u_\infty$, and the axial mean u/u_∞, and fluctuating u'/u_∞ velocity contours) over an oscillation cycle for $\alpha(t) = 18$ deg $+ 6$ deg $\sin \omega t$ and $\kappa = 0.09$ at $x/c = 1$ is illustrated in Fig. 3. Also shown in Fig. 3 are the results of a stationary wing positioned at $\alpha = 10$–19 deg with a static-stall angle α_{ss} of 14.5 deg. It is evident that the wing oscillation imposed a strong discrepancy in contour shapes and magnitudes between the pitch-up and pitch-down phases of an oscillation cycle. The qualitative behavior of the tip vortex, corresponding to both the prior to, during, and after stall flow regimes, or conditions, can be depicted next. The prior-to-stall quasi-steady flow condition consisted of two parts:

1) For $\alpha_u = 12$ deg up to about α_{ss} during pitch-up, the boundary-layer flow remained attached, especially over the inboard regions of the wing, which rendered a less turbulent and better organized tip vortex of slightly weaker circulation, compared to their static counterparts.

2) For $\alpha_u \approx \alpha_{ss}$ to about 22 deg, the vortex was observed to be more diffusive and had a higher vortex strength (compared to 1) because of the presence of the turbulent trailing-edge flow reversal and the formation and growth of the LEV on the wing upper surface. During stall (covering $\alpha_u \approx 22$ deg to $\alpha_d \approx 20$ deg), the massive flow separation (over the entire wing upper surface as a result of LEV detachment) leading to the loss of vortex axisymmetry with a sharp decreased vortex strength, accompanied by an increased axial velocity and turbulence level, can be seen from the ζ, u, and u' isocontour maps. During the after-stall pitch-down condition (covering $\alpha_d \approx 20$ to 13 deg), the tip vortex was of much lower vorticity and became more organized (because of the reattachment of the largely separated turbulent flow onto the wing upper surface), compared to the same range of $\alpha(t)$ during pitch-up as well as a stationary wing at the same incidence.

Figure 3 also indicates that during pitch-down, the vortex regions suffered from velocity deficit, in contrast to a stationary wing at the same α for which the u/u_∞ contours exhibited islands of wake- and jet-like axial velocity distributions. Note that according to Bachelor,[13] the magnitude of the axial velocity in a trailing vortex can be determined from a balance between the energy loss caused by dissipation in the wing boundary layer and the radial gradient in the circulation strength. It is shown later that except in the vicinity of α_{max}, the velocity deficit and wake width were found to be decreased and increased with $\alpha(t)$, respectively, as a result of the largely separated flow from the wing upper surface, during pitch-down compared with during pitch-up. Details of the crossflow vectors and the contours of $\zeta c/u_\infty$, u/u_∞, and u'/u_∞ for $\alpha_u = \alpha_d = 13$, 18, and 22 deg at $x/c = 1$ were regenerated and are given in Fig. 4. These specific angles of attack were selected to illustrate the representative tip-vortex flow structures corresponding to the just-mentioned various flow conditions, involving attached flow, flow reversal and LEV growth, LEV detachment, and flow reattachment, which occurred on a wing undergoing deep-stall oscillations. The stationary-wing results are also included for comparisons. The distribution and variation of the phase-locked ensemble-averaged vortex flow quantities (e.g., the tangential velocity v_θ, ζ, u, and u') across the vortex over an oscillation cycle are presented later.

Figure 4a shows that at $\alpha_u = 13$ deg (i.e., part 1 flow regime as just described), as expected, the flow consisted of a small concentrated vortex core (of a radius of $0.075c$) surrounded by a circulating velocity field that wound the rest of the wing wake into an ever-increasing spiral. The flow outboard of the wing followed nearly a circumferential path about the vortex center; however, inboard, there was a stronger radial flow away form the vortex center. The dashed lines denote the instantaneous location of the wing trailing edge. The vortex was less tightly wound and had a slightly lower maximum tangential velocity and a much decreased core vorticity, compared to a stationary wing at 13 deg (Figs. 5a, 5b, 6a, and 6b). Both v_θ and ζ across the inner region of the vortex varied considerably during the oscillation cycle and had a significantly higher value during pitch-up than during pitch-down (e.g., compared to $\alpha_d = 13$ deg during the pitch-down flow reattachment process). No significant variation in the core radius r_c and outer radius r_o of the vortex during pitch-up, compared to a stationary wing, was observed; both r_c and r_o, however, increased drastically above the stationary-wing values during pitch-down at $\alpha_d = 13$ deg (Fig. 6c). Note that the core radius was defined by the location of the maximum induced tangential velocity

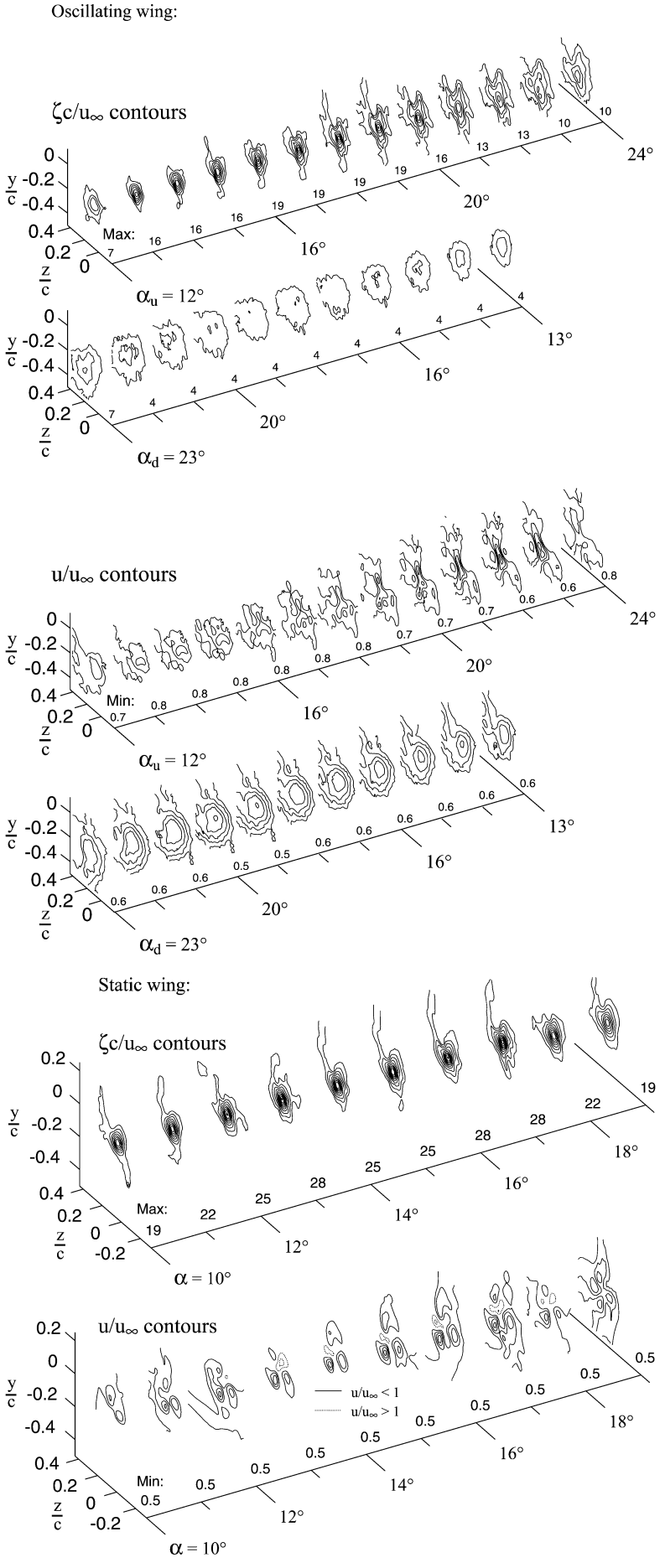

Fig. 3 Composite plots of nondimensional phase-locked ensemble-averaged vortex flow contours at $x/c = 1.0$.

and the outer radius defined by the extent at which the circulation $\Gamma(r_o)$ was 98% of the total circulation Γ_0. The axial velocity at $\alpha_u = 13$ deg was wake like (Fig. 5c), in contrast to a stationary wing at the same airfoil incidence for which islands of axial velocity both fell behind and exceeded the freestream value. At $\alpha_u = 13$ deg, the u' distribution remained similar to a stationary wing but the location of the peak turbulence coincided with the vortex center (identified by the location of maximum vorticity). Figure 4a also indicates that outside the vortex core region, the axial turbulence structure was clearly dominated by the wake spiral. The spiral (corresponding to the shear layer from the inboard regions of the flow, which was in a process of rolling up to form the axial tip vortex) was generally more organized for the most part during pitch-up than during pitch-down. At $\alpha_d = 13$ deg during the pitch-down flow reattachment process, the tip vortex was more diffused (i.e., of increased r_c and r_o) with a decreased v_θ, rendering a lower vorticity and circulation (due to the agitated flow separation) compared to $\alpha_u = 13$ deg as well as a stationary wing at the same α. A wider and well-defined axial wake profile (resembled that of a circular cylinder) of higher u' was also observed at $\alpha_d = 13$ deg.

At $\alpha_u = 18$ deg ($>\alpha_{ss}$) during pitch-up (i.e., in the aforementioned part 2 flow regime), the vortex remained axisymmetric with less concentrated vorticity distributions (as a result of the significant delay of the flow separation compared to their stationary counterparts), as can be clearly seen from the crossflow velocity vectors and the vorticity contour maps (Fig. 4b). The magnitude of the cross-stream velocity vectors at $\alpha_u = 18$ deg was of the order of u_∞ and was, therefore, quite significant. The tangential velocity gradient remained linear in the core regions (Fig. 5a) and was much steeper during pitch-up than during pitch-down at $\alpha_d = 18$ deg, which resulted in a smaller vortex size (Fig. 5c) and a lower core vorticity distribution during pitch-up (Fig. 5b). During pitch-down at $\alpha_d = 18$ deg, the peak values of v_θ and ζ were found to be considerably lower compared to $\alpha_u = 18$ deg as well as a stationary wing at the same α; the vortex size was, however, found to be larger instead. Note that at $\alpha_d = 18$ deg during pitch-down flow reattachment the flow was highly agitated

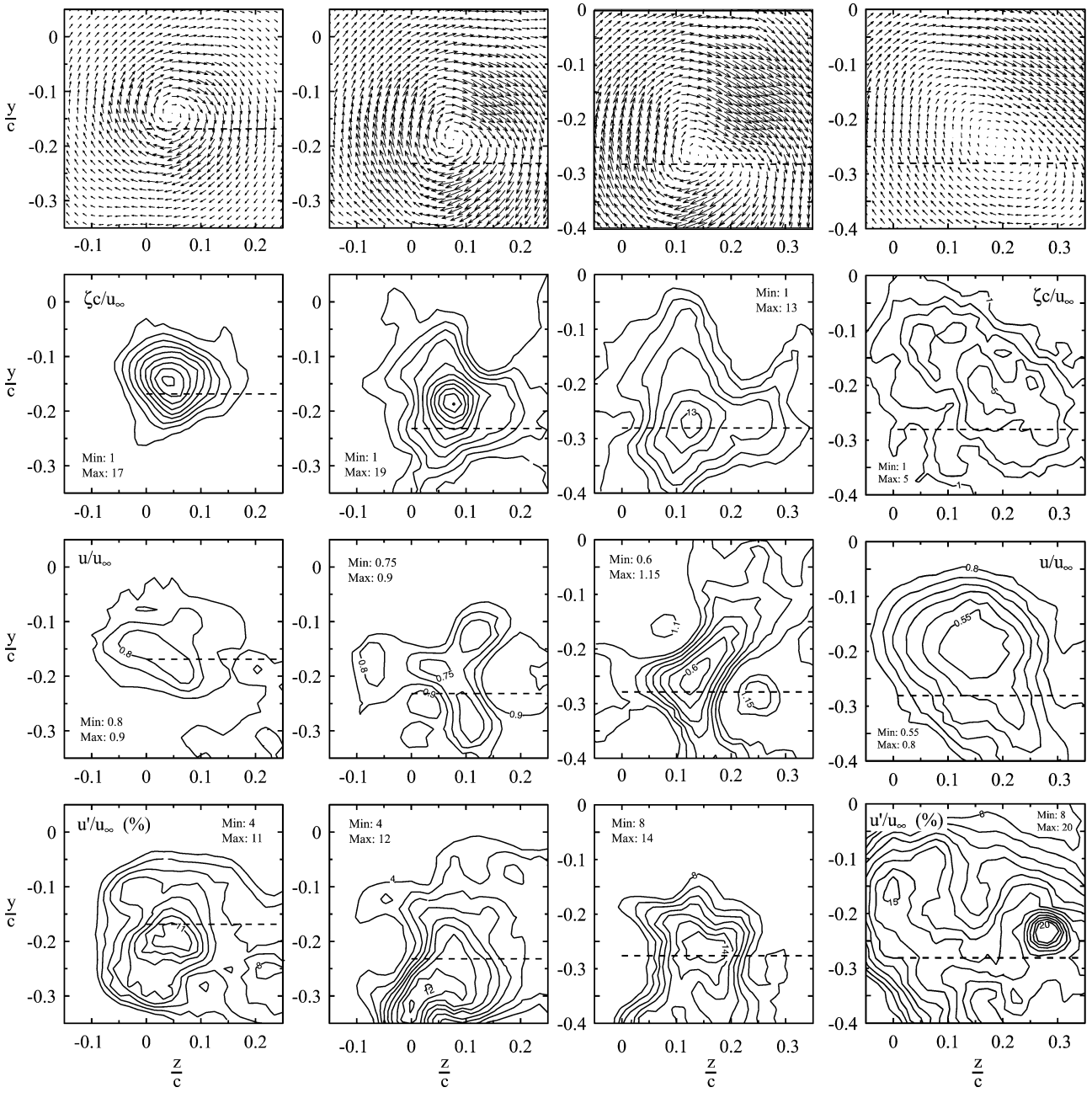

a) $\alpha_u = 13$ deg **b) $\alpha_u = 18$ deg** **c) $\alpha_u = 22$ deg** **d) $\alpha_d = 22$ deg**

Fig. 4 Nondimensional phase-locked ensemble-averaged vortex flow structures at $x/c = 1$. Numerical values denote $\zeta c/u_\infty$, u/u_∞, and u'/u_∞ levels with constant increments of 2, 0.05, and 1, respectively.

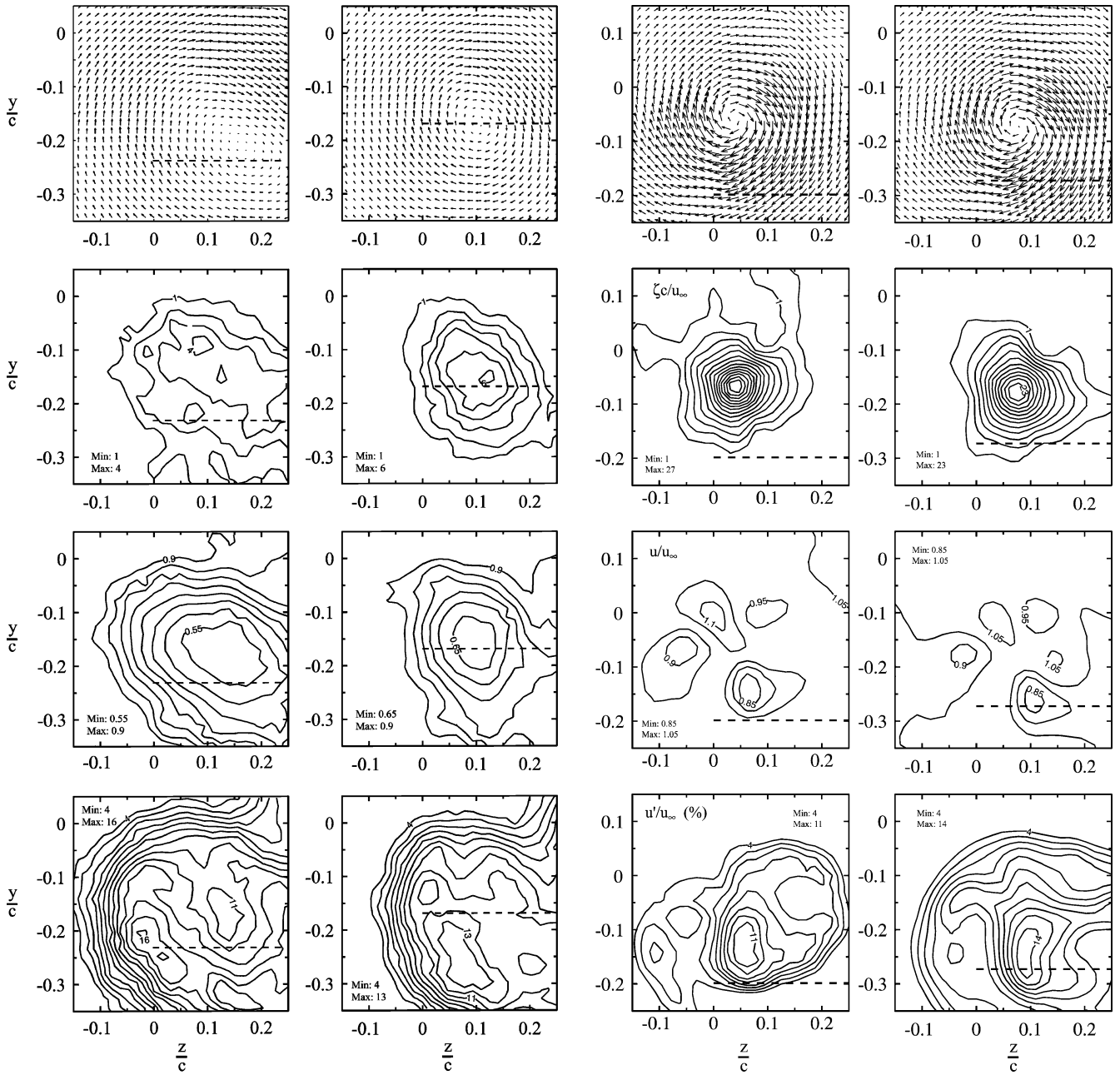

e) $\alpha_d = 18$ deg **f) $\alpha_d = 13$ deg** **g) $\alpha_{static} = 13$ deg** **h) $\alpha_{static} = 18$ deg**

Fig. 4 Nondimensional phase-locked ensemble-averaged vortex flow structures at $x/c = 1$. Numerical values denote $\zeta c/u_\infty$, u/u_∞, and u'/u_∞ levels with constant increments of 2, 0.05, and 1, respectively (continued).

mostly because of the reattaching of the largely separated turbulent boundary layer onto the suction side of the wing, which fed into the vortex and resulted in a drastically reduced ζ and v_θ and an increased r_c, r_o, u_c, and u'. The peak values of $v_{\theta\text{peak}}/u_\infty$, $\zeta_{\text{peak}}c/u_\infty$, u_c/u_∞, r_c/c, and r_o/c at $\alpha_u = 18$ deg ($\alpha_d = 18$ deg) were foung to be 0.64 (0.32), 21 (4), 0.75 (0.525), 0.12 (0.175), and 0.16 (0.24), respectively, compared to 0.66, 27.5, 1.08, 0.075, and 0.12, respectively, of a stationary wing positioned at 18 deg.

At $\alpha_u = 22$ deg during pitch-up (i.e., immediately before the ultimate growth of the LEV to the full chord length and its subsequent detachment from the wing upper surface), the entrainment of the highly rotational LEV flow into the tip vortex resulted in a more diffused and lowered peak vorticity distribution and an increased r_c and r_o, compared to $\alpha_u = 18$ deg. An axial flow of both wake- and jet-like velocity profiles, similar to that of a stationary wing, was observed (denoted Δ symbols in Fig. 5c). On the other hand, at $\alpha_d = 22$ deg during pitch-down (i.e., in the during-stall flow regime), the flow separated from the entire wing upper surface and resulted in an elliptical and high diffused tip vortex accompanied by an increased wake width and turbulence level, compared to at $\alpha_u = 22$ deg during pitch-up. No noticeable difference in the wake velocity deficit was, however, observed between $\alpha_u = 22$ and $\alpha_d = 22$ deg.

Figures 6a–6e summarize the dynamic loops of the nondimensional $v_{\theta\text{peak}}$, ζ_{peak}, u_c, and r_c and r_o, as well as the vortex trajectory at $x/c = 1$ over an oscillation cycle. Note that because of the convection time required for a tip-vortex flow structure to propagate from the wing to the downstream location of the sensor there is a phase lag between any instantaneous sensor reading and the position of the wing at that instant, and so it is necessary to discuss briefly the phase-lag compensation employed in the present study before the discussion of the dynamic loops displayed in Fig. 6. Figure 7 shows both the uncompensated and compensated dynamic-circulation loops for $\alpha(t) = 18 \text{ deg} + 6 \text{ deg} \sin \omega t$ and $\kappa = 0.09$ at $x/c = 1$. By assuming that within the streamwise length scale considered, any streamwise distortion of the flow structure that occurs

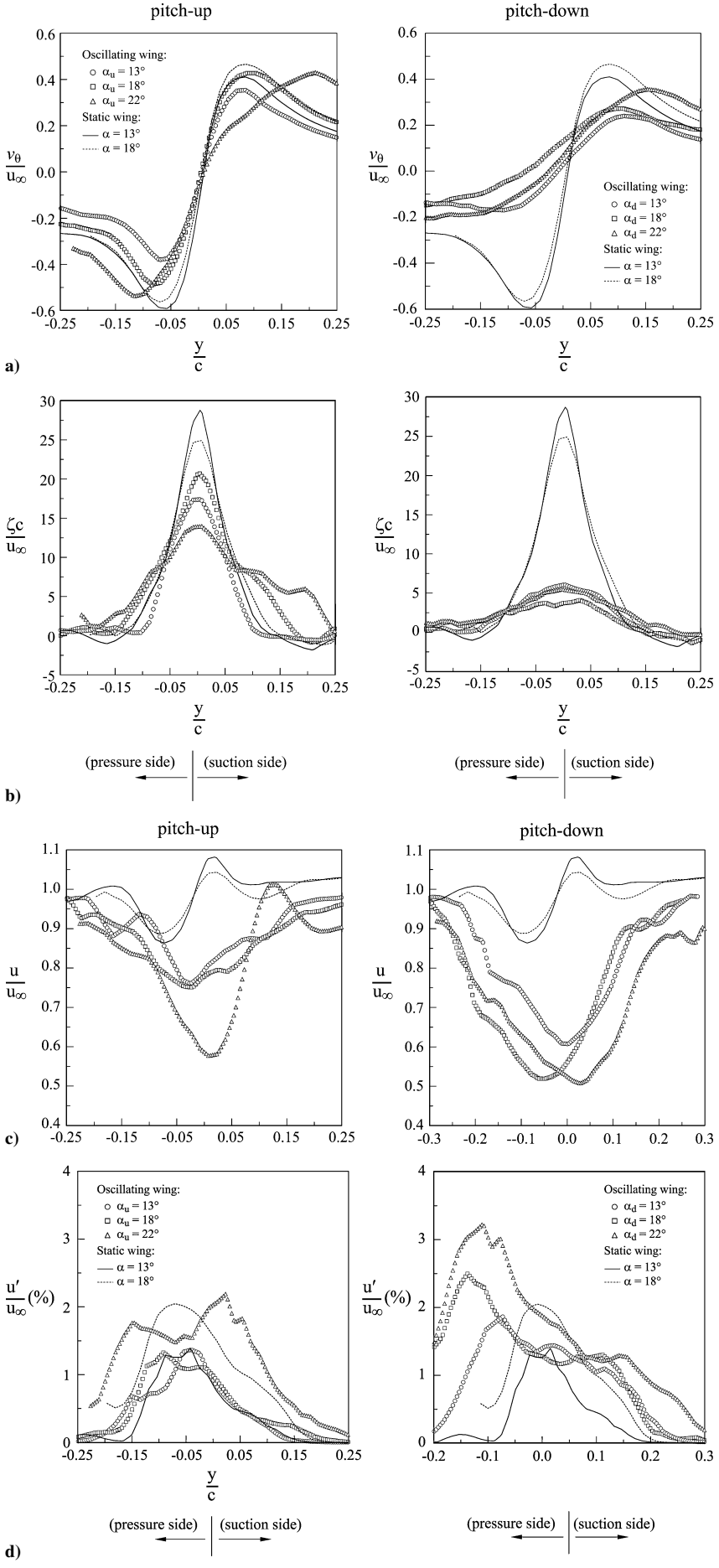

Fig. 5 Distributions of phase-locked ensemble-averaged vortex flow quantities across the vortex at $x/c = 1$.

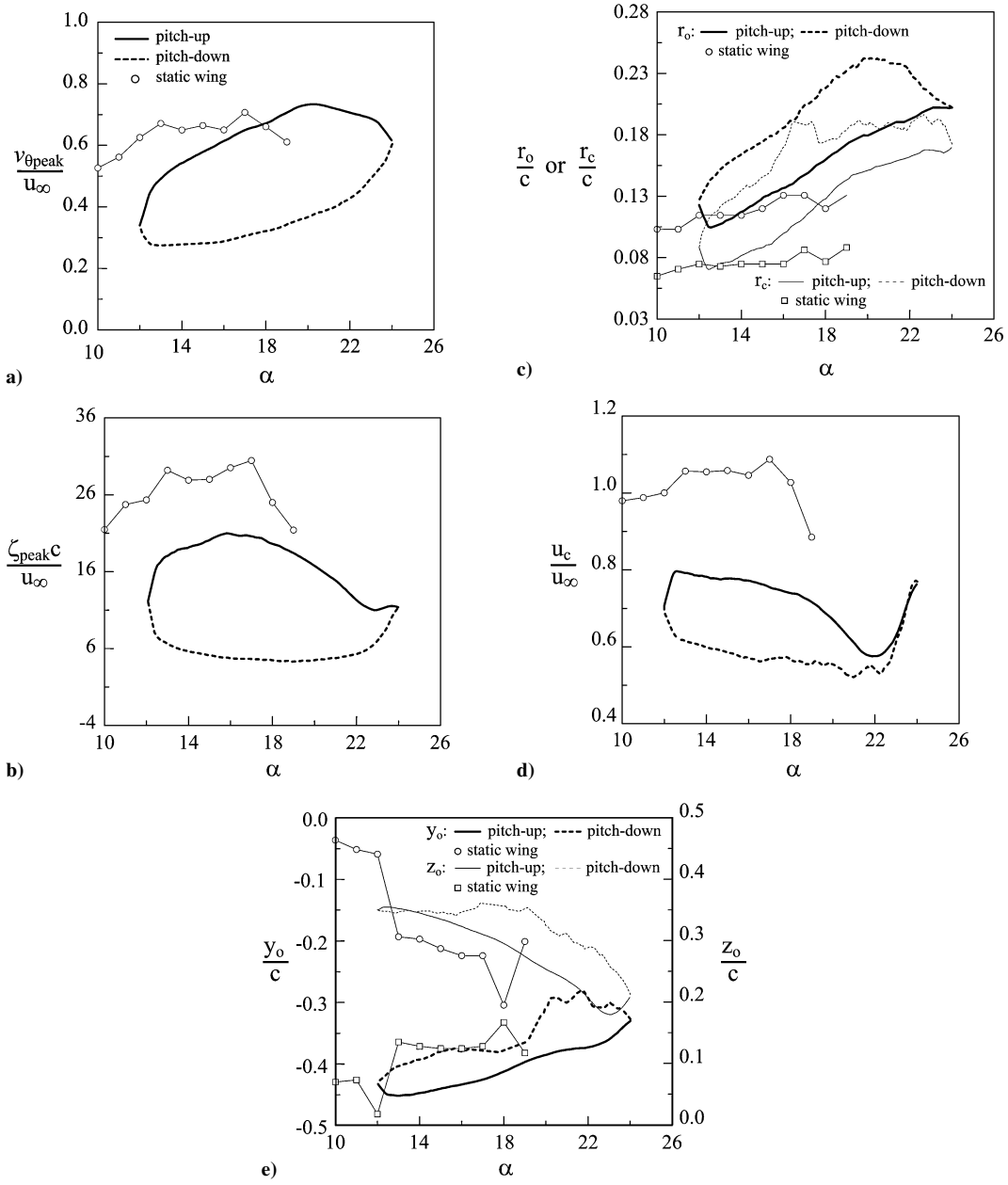

Fig. 6 Dynamic loops of peak vortex flow qualities over an oscillation cycle at $x/c = 1$.

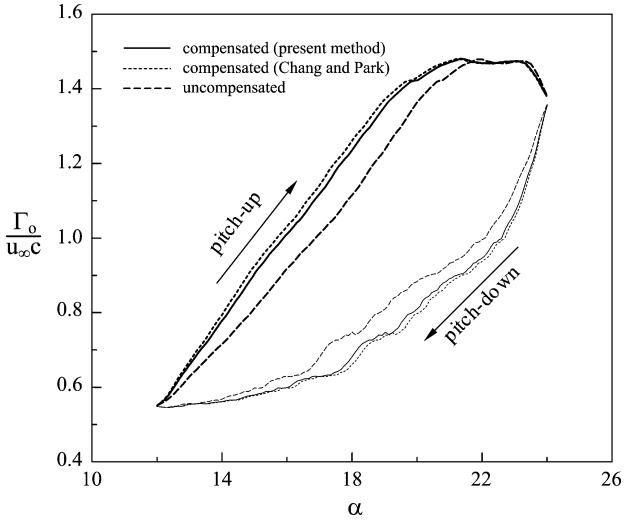

Fig. 7 Phase-lag compensation.

is negligible, and that the convection speed u_{conv} is constant, then the angle of attack through which the wing has swept during the convection time can be directly calculated if u_{conv} can then be approximated. An upper and lower bound is subsequently imposed upon the convection speed because it cannot fall outside of the range of axial velocities measured within the volume through which it has moved. In the present experiment, u_{conv} was approximated as the upper-bound freestream speed because it resulted in the smallest phase lag correction and, by extension, a more conservative result. The phase-lag compensation scheme suggested by Chang and Park,[9] in which u_{conv} was approximated with a spatial average axial velocity in the vicinity of the vortex center, was also included in Fig. 7. Note that because some of the measured axial velocities appeared to exceed the freestream limit, Chang and Park's compensation scheme could, therefore, somewhat inflate the convection speed. The measurements reported in this study were phase-lag compensated by letting $u_{conv} = u_\infty$. Typical uncompensated and compensated angles of attack at $x/c = 1$ are listed in Table 1.

Figure 6a indicates that $v_{\theta peak}$ increased with $\alpha(t)$ and was found to be significantly higher during pitch-up than during pitch-down. A local maximum and minimum of $73\%u_\infty$ and $28\%u_\infty$ at $\alpha_u = 20$ deg

(corresponding to the sudden breakdown of the turbulent flow in the inboard of the wing) and $\alpha_d = 13$ deg (corresponding to the end of the downstream spread of the reattachment), respectively, were obtained. The rate of increase and decrease of $dv_{\theta peak}/d\alpha$ during both pitch-up and pitch-down, except in the vicinity of α_{max} and α_{min}, were observed to be linear and remained constant with a $dv_{\theta peak}/d\alpha$ of about 0.033 per degree. Note that because of the asymmetry of the vortex flow during the during-stall flow condition (e.g., in the vicinity of α_{max}) the values of $v_{\theta peak}$ and r_c and r_o were circumferentially averaged and can only therefore serve as a qualitative reference. The vorticity inside the core reached a maximum value (of $\zeta_{peak}c/u_\infty = 22$) at 16 deg during pitch-up (corresponding to the onset of the flow reversal), while remaining a virtually constant value of $\zeta_{peak}c/u_\infty = 5$ during pitch-down flow reattachment from $\alpha_d = 22$ to 13 deg (Fig. 6b). Similar to the variation of $v_{\theta peak}$ with $\alpha(t)$, r_c and r_o also exhibited a linear increase (up to the LEV detachment) but had a higher value during pitch-down than during pitch-up

Table 1 Uncompensated and compensated α at $x/c = 1$

Pitch-up		Pitch-down	
Uncompensated	Compensated	Uncompensated	Compensated
12	12.00	24	24.13
13	12.74	23	23.38
14	13.51	22	22.61
15	14.30	21	21.79
16	15.13	20	20.93
17	16.02	19	20.01
18	16.97	18	19.03
19	17.99	17	17.98
20	19.07	16	16.87
21	20.21	15	15.70
22	21.40	14	14.50
23	22.62	13	13.26
24	23.87	12	12.00

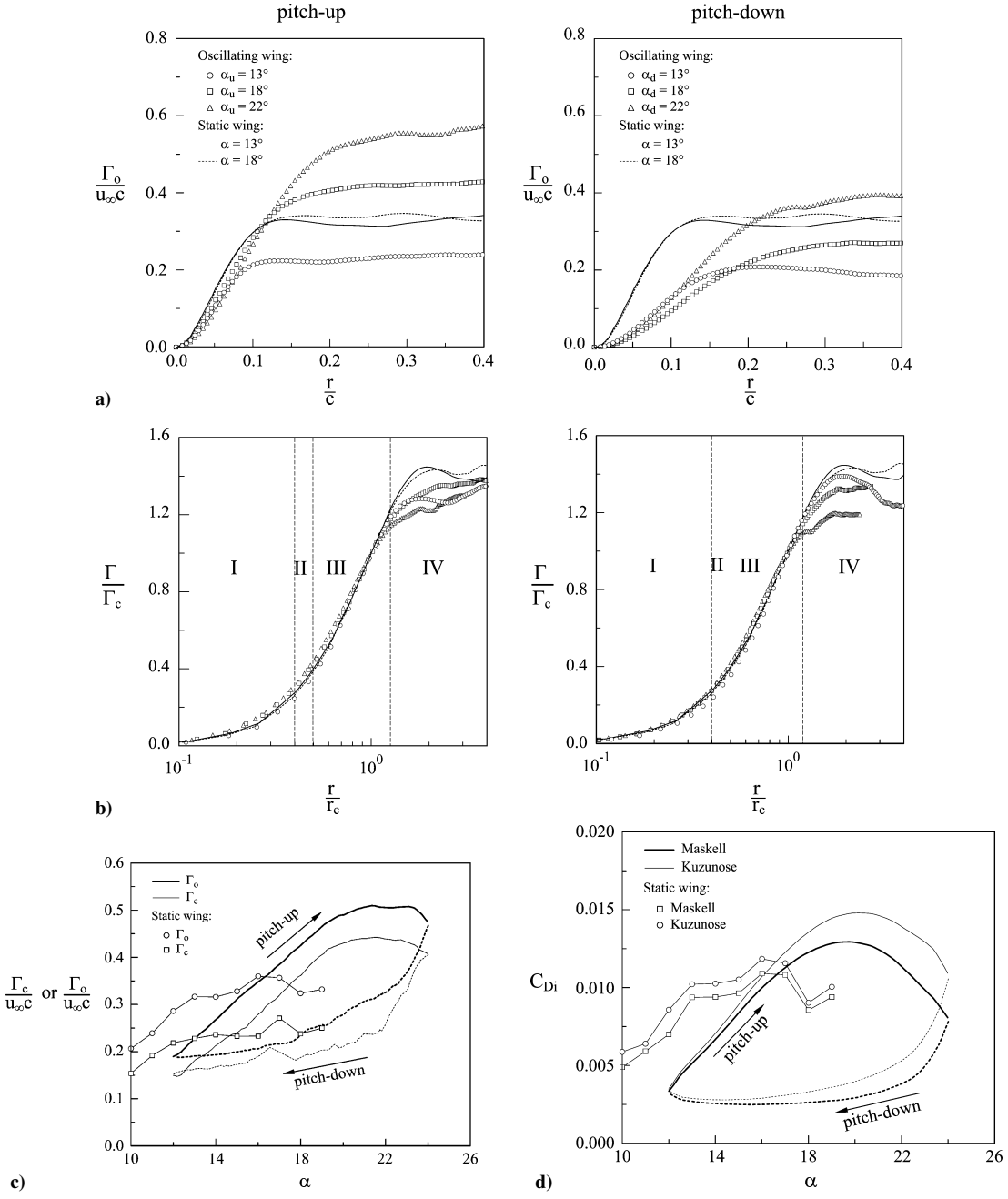

Fig. 8 Circulation and lift-induced drag coefficient: I, inner-core region; II, buffer region; III, logarithmic region; and IV, outer region.

(Fig. 6c). A constant growth rate of about $\mathrm{d}(r_o/c)/\mathrm{d}\alpha = 0.0129$ and $\mathrm{d}(r_c/c)/\mathrm{d}\alpha = 0.0117$ was obtained. The wakelike core axial velocity, or velocity deficit, however, was found to decrease with $\alpha(t)$ and exhibited a much lower value during pitch-down than during pitch-up (Fig. 6d). A local minimum u_c of $0.6u_\infty$ at $\alpha_u = 22$ deg during pitch-up (corresponding to the pass-off of the LEV of the wing trailing edge and the onset of the dynamic stall), followed by a sharp rise and drop in the velocity deficit for $\alpha_u = 22$ deg to $\alpha_d = 22$ deg, was noticed.

Figure 6e summarizes the movement of vortex center relative to the wing tip at the trailing edge during the oscillation cycle (y_o/c and z_o/c vs α) at $x/c = 1$. The vortex center moved slightly outboard from the wing tip and downward relative to the trailing edge as α increased over the oscillation cycle; an opposite movement of the vortex center was observed as α was decreased. The vortex center seemed to extend much farther outboard during pitch-down, implying that much of the circulation and the spanwise lift distribution was shed, or shifted, outboard in the sheet and resulted in a weaker circulation (Fig. 8).

B. Circulation and Lift-Induced Drag

Figure 8a shows the variation of the circulation $\Gamma(r)/u_\infty c$ with radius r/c at $\alpha_u = 13$, 18, and 22 deg, and $\alpha_d = 13$, 16, and 19 deg. Also shown in this figure are the results of a stationary wing at $\alpha = 13$ and 18 deg. The gradual and monotonic increase in circulation with r of an oscillating wing was similar to a stationary wing.[12] Outside the inner-flow region, Γ varied considerably during the oscillation cycle, and the individual distributions for a given α during pitch-up and pitch-down motion did not correspond with each other. Furthermore, by normalizing $\Gamma(r)$ by the core circulation Γ_c and plotting against $\log(r/r_c)$, it is evident that except for the LEV-detachment flow regime (i.e., for $\alpha_u = 22$ deg to $\alpha_d = 22$ deg) the distribution of circulation within the tip vortex core followed a $\Gamma \propto r^2$ profile for $r/r_c < 0.4$ and varied logarithmically for $0.5 < r/r_c < 1.2$ (Fig. 8b); a phenomenon similar to that of a stationary wing.[12,14] For $r/r_c > 1.2$ (denoted by region IV), the value of Γ continued to vary with r as a result of the slow addition of vorticity to the outer layers of the vortex from the shear layer arriving from the inboard regions. The empirical curve-fit relationships that describe the inner-core region and the region where the $\Gamma(r)$ distribution is logarithmic, according to Hoffman and Joubert[15] and Phillips,[16] are

$$\Gamma(r)/\Gamma_c = A(r/r_c)^2 \qquad \text{for} \qquad r/r_c < 0.4 \tag{1}$$

$$\Gamma(r)/\Gamma_c = B\log(r/r_c) + C \qquad \text{for} \qquad 0.5 < r/r_c < 1.2 \tag{2}$$

The curve-fit constants obtained are listed in Table 2. Furthermore, all of the data within $0 < r/r_c < 1.2$ collapsed together onto a sixth-order polynomial[12,14] with a self-autocorrelation coefficient of 0.998:

$$\Gamma(r)/\Gamma_c = 1.756(r/r_c)^2 - 1.044(r/r_c)^4 + 0.263(r/r_c)^6 \tag{3}$$

Figure 8c shows the dynamic loops of the total $\Gamma_0/u_\infty c$ and core $\Gamma_c/u_\infty c$ circulation over an oscillation cycle at $x/c = 1$, which clearly demonstrate the significant hysteretic property existing between pitch-up and pitch-down (similar to the dynamic C_l loop shown in Fig. 1). Both Γ_c and Γ_0 increased with $\alpha(t)$. During pitch-up, a significantly higher circulation was observed compared to during pitch-down (because of the massive flow separation, as a result of the LEV detachment and the subsequent flow reattachment process). The Γ values were lower than the stationary-wing values during the pitch-down and during the initial part of the pitch-up. Both Γ_0 and Γ_c increased linearly up to $\alpha_u = 21$ deg during pitch-up, reached a local maximum (with $\Gamma_0/u_\infty c = 0.51$ and $\Gamma_c/u_\infty c = 0.44$) for $\alpha_u = 21$–23 deg, and were followed by a continuous drop until $\alpha_d = 18$ deg. It is significant to note that the rate of increase of Γ_0 and Γ_c per unit α during pitch-up, except in the vicinity of $\alpha_{\max}$, was found to be $\mathrm{d}(\Gamma_0/u_\infty c)/\mathrm{d}\alpha = \mathrm{d}(\Gamma_c/u_\infty c)/\mathrm{d}\alpha = 0.033$ per degree, which is similar to the growth rate of the peak tangential velocity with $\alpha(t)$ [i.e., $\mathrm{d}(v_{\theta\mathrm{peak}}/u_\infty)/\mathrm{d}\alpha = 0.033$] during pitch-up.

Finally, the phase-locked ensemble-averaged lift-induced drag coefficient C_{Di} ($=D_i/\frac{1}{2}\rho_\infty u_\infty^2 S$, where D_i is the induced drag force) was also computed, based on the vorticity inferred from the measured velocity field, by using the Maskell induced-drag model[17] at $x/c = 1$. The vw-crossflow velocity vectors within the measurement plane were decomposed into a stream function $\psi(y,z)$ and a velocity potential $\phi(y,z)$ with the imposed boundary conditions requiring both ψ and ϕ to be zero on the edges of the measurement plane. The induced drag was then obtained by

$$D_i = \frac{1}{2}\rho_\infty \iint_{S_\zeta} \psi\zeta \,\mathrm{d}y\,\mathrm{d}z - \frac{1}{2}\rho_\infty \iint_{S1} \phi\sigma \,\mathrm{d}y\,\mathrm{d}z \tag{4}$$

where ζ is the vorticity, the surface S_ζ is the region within S1 where the vorticity is nonzero, σ $(= \partial v/\partial y + \partial w/\partial z)$ is a source term, and the flow is incompressible. Figure 8d shows that, similar to the observed trend in Γ, the values of C_{Di} were found to increase linearly with α up to $\alpha_u \approx 20$ deg during pitch-up (with a local maximum $C_{\mathrm{Di}} = 0.013$), followed by a decrease for $\alpha_u = 20$ deg to $\alpha_d = 20$ deg. The C_{Di}, however, remained basically unchanged ($C_{\mathrm{Di}} = 0.0025$) during the pitch-down flow reattachment process ($\alpha_d = 20$ deg $- 13$ deg). The rate of increase of C_{Di} per unit α was much higher during pitch-up than during pitch-down. The minima in the C_{Di} loops generally occurred when the circulation was weakest, or at smallest $\alpha(t)$. The maxima in the C_{Di} loops occurred when the tip vortex was strongest, which, notably, was not at the maximum α.

Table 2 Curve-fit constants of Eqs. (1) and (2) for an oscillating wing

$x/c = 1$				$\alpha_u = 18$ deg			
$\alpha(t)$, deg	A	B	C	x/c	A	B	C
$\alpha_u = 13$	1.727	1.969	0.994	1	1.393	2.215	0.946
$\alpha_u = 18$	1.574	1.985	0.955	1.5	1.566	2.230	0.994
$\alpha_u = 22$	1.666	2.010	0.972	2	1.667	2.110	0.974
$\alpha_d = 19$	1.566	2.230	0.994	2.5	1.786	1.942	0.962
$\alpha_d = 16$	1.619	1.197	0.978	3	1.611	2.208	0.997
$\alpha_d = 13$	1.811	2.154	0.986	——	——	——	——

C. Variation of Vortex Flow Quantities and C_{Di} with x/c

The variation of the nondimensional vortex flow quantities and C_{Di} with the downstream distance ($x/c = 0.5$–3) over an oscillation cycle is illustrated in Fig. 9. The $v_{\theta\mathrm{peak}}$ and ζ_{peak} (r_c and r_o) had higher (lower) magnitudes during pitch-up (pitch-down) than during pitch-down (pitch-up), regardless of x/c. The peak tangential velocity was, however, found to decrease with the downstream distance (for $x/c > 1.5$) and increase with $\alpha(t)$ (Fig. 9a). No noticeable variation in r_c and r_o was observed with increasing x/c during pitch-up (Figs. 9b and 9c); the vortex size was found to increase with the downstream distance during pitch-down. The degree of asymmetry, or hysteresis, in $v_{\theta\mathrm{peak}}$ (r_c and r_o) was found to be a weaker (stronger) function of x/c. The magnitudes of the core vorticity were insensitive to x/c during pitch-down, but decreased rather significantly with the downstream distance during pitch-down (Fig. 9d). For $x/c > 1$, the axial velocity distributions were wake like during the entire oscillation cycle. The spatial-temporal variation of Γ and C_{Di} over an oscillation cycle are displayed in Figs. 9e–9g. Both Γ_c and Γ_0 increased with $\alpha(t)$ and had a higher value during pitch-up than during pitch-down and were relatively insensitive to x/c, especially during the pitch-up motion (Figs. 9e and 9f). Figure 9g indicates that a significant increase in C_{Di} during pitch-up at $x/c = 0.5$ was observed. Only small variation in C_{Di} with x/c was noticed for $x/c > 0.5$.

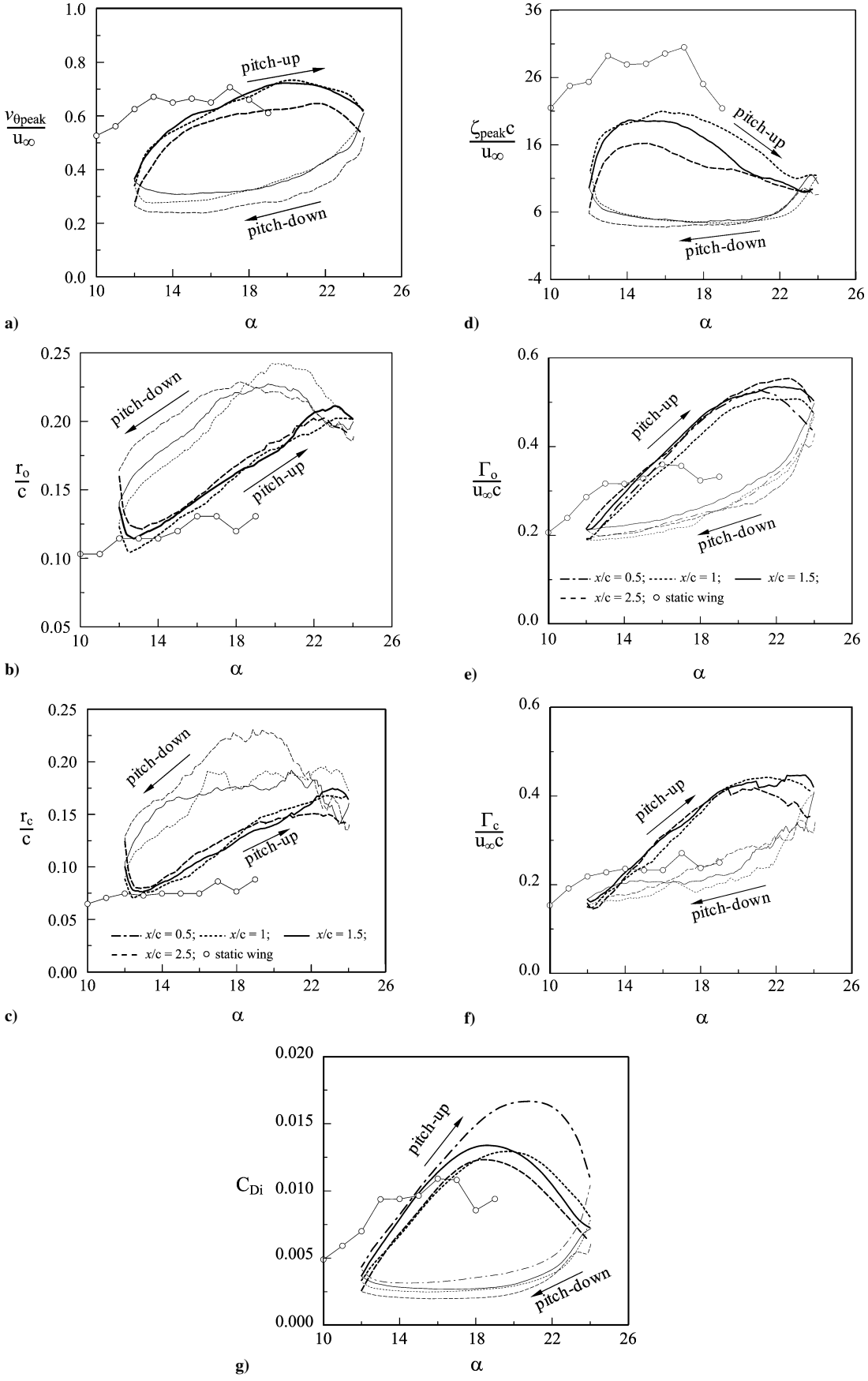

Fig. 9 Variation of vortex flow quantities and C_{Di} with x/c.

IV. Conclusions

The near-field tip-vortex flow quantities of a rectangular NACA 0015 wing undergoing deep-stall oscillations were investigated. The wing oscillation imposed a strong discrepancy in contour shapes and magnitudes between the pitch-up and pitch-down phases of the oscillation cycle. The vortex was more organized and nearly axisymmetric (for $x/c > 0.5$) during pitch-up motion than during the pitch-down motion, except in the vicinity of $\alpha_{\max}$. The tangential velocity and circulation increased with $\alpha(t)$ and decreased slightly with x/c and had higher magnitudes during pitch-up than during pitch-down. The vortex size increased with $\alpha(t)$ and was larger during pitch-down than during pitch-up. The vortex size was also observed to increase with x/c during pitch-down while remaining unchanged with x/c during pitch-up. The axial velocity distribution across the vortex was always wake like during pitch-down and decreased with $\alpha(t)$, followed by a significant increase and decrease in the vicinity of $\alpha_{\max}$. The normalized circulation within the inner region of the nearly axisymmetric tip vortex exhibited a self-similar structure. Both circulation and C_{Di} had higher magnitudes during pitch-up than during pitch-down, and varied insignificantly with the downstream distance.

Acknowledgment

This work was supported by the Natural Sciences and Engineering Research Council of Canada.

References

[1]McCroskey, W. J., Carr, L. W., and McAlister, K. W., "Dynamic Stall Experiments on Oscillating Airfoils," *AIAA Journal*, Vol. 14, No. 1, 1976, pp. 57–63.

[2]Carr, L. W., McAlister, K. W., and McCroskey, W. J., "Analysis of the Development of Dynamic Stall Based on Oscillating Airfoil Experiments," NASA TN D-8382, 1979.

[3]McCroskey, W. J., "Unsteady Airfoils," *Annual Review of Fluid Mechanics*, Vol. 14, 1982, pp. 285–311.

[4]Ericsson, L. E., and Reding, J. P., "Fluid Mechanics of Dynamic Stall. Part I. Unsteady Flow Concept," *Journal of Fluids and Structures*, Vol. 2, No. 1, 1988, pp. 1–33.

[5]Lee, T., and Basu, S., "Measurement of Unsteady Boundary Layer Developed on an Oscillating Airfoil Using Multiple Hot-Film Sensors," *Experiments in Fluids*, Vol. 25, No. 2, 1998, pp. 108–117.

[6]Lee, T., and Gerontakos, P., "Investigation of Flow over an Oscillating Airfoil," *Journal of Fluid Mechanics*, Vol. 512, 2004, pp. 313–341.

[7]Freymuth, P., Finaish, F., and Bank, W., "Visualization of Wing-Tip Vortices in Accelerating and Steady Flow," *Journal of Aircraft*, Vol. 23, No. 9, 1985, pp. 730–733.

[8]Ramaprian, B. R., and Zheng, Y., "Near Field of the Tip Vortex Behind an Oscillating Rectangular Wing," *AIAA Journal*, Vol. 36, No. 7, 1998, pp. 1263–1269.

[9]Chang, J. W., and Park, S. O., "Measurement in the Tip Vortex Roll-up Region of an Oscillating Wing," *AIAA Journal*, Vol. 38, No. 6, 2000, pp. 1092–1095.

[10]Wenger, C. W., and Devenport, W. J., "Seven-Hole Pressure Probe Calibration Utilizing Look-Up Error Tables," *AIAA Journal*, Vol. 37, No. 6, 1999, pp. 675–679.

[11]Chow, J. S., Zilliac, G. G., and Bradshaw, P., "Mean and Turbulence Measurements in the Near Field of a Wingtip Vortex," *AIAA Journal*, Vol. 35, No. 10, 1997, pp. 1561–1567.

[12]Birch, D., and Lee, T., "Structure and Induced Drag of a Tip Vortex," *Journal of Aircraft*, Vol. 41, No. 5, 2004, pp. 1138–1145.

[13]Batchelor, G. K., "Axial Flow in Trailing Line Vortices," *Journal of Fluid Mechanics*, Vol. 20, 1964, pp. 645–658.

[14]Ramaprian, B. R., and Zheng, Y., "Near Field of the Tip Vortex Behind an Oscillating Rectangular Wing," *AIAA Journal*, Vol. 36, No. 7, 1998, pp. 1263–1269.

[15]Hoffmann, E. R., and Joubert, P. N., "Turbulent Line Vortices," *Journal of Fluid Mechanics*, Vol. 16, 1963, pp. 395–411.

[16]Phillips, W. R. C., "The Turbulent Trailing Vortex During Roll-Up," *Journal of Fluid Mechanics*, Vol. 105, 1981, pp. 451–467.

[17]Maskell, E., "Progress Towards a Method for the Measurement of the Components of the Drag of a Wing of Finite Span," RAE TR 72232, 1973.

H. Reed
Associate Editor